IEEE Access
Multidisciplinary | Rapid Review | Open Access Journal

Received January 2, 2020, accepted January 14, 2020, date of publication January 20, 2020, date of current version January 31, 2020.

Digital Object Identifier 10.1109/ACCESS.2020.2968109

Correlation Between Thermal Parameters and Morphology of Cross-Linked Polyethylene

YIFENG ZHAO[1], ZHUOZHAN HAN[1], YUE XIE[1], XINGHUI FAN[1], YANGYANG NIE[1], PENGYU WANG[1], GANG LIU[1], (Member, IEEE), YANPENG HAO[1], (Member, IEEE), JIASHENG HUANG[2], AND WENWEI ZHU[3]

[1]School of Electric Power Engineering, South China University of Technology, Guangzhou 510630, China
[2]Transmission Management Office, Guangzhou Power Supply Bureau, Guangzhou 510640, China
[3]Planning research center, Guangdong Power Grid Corporation, Guangzhou 510640, China

Corresponding authors: Gang Liu (liugang@scut.edu.cn) and Yanpeng Hao (yphao@scut.edu.cn)

This work was supported in part by the Foundation Item: Technical Projects of China Southern Power Grid under Grant GDKJXM20172797.

ABSTRACT This paper reveals a correlation between morphology and thermal parameters on cross-linked polyethylene (XLPE) cable with different insulating states. Several cables were selected to detect the physicochemical and thermal parameters of the XLPE. The results show that the cable ampacity is determined by the thermal parameters, which are deeply subjected to the morphology of the XLPE. The molecular chain and crystal structure of the XLPE have a close connection with the thermal resistivity. The physicochemical parameters of carbonyl index (*CI*) and unsaturated band index (*UBI*) from Fourier transform infrared spectrum (FTIR) and melting range (R_m) from differential scanning calorimetry (DSC) can be the indicator to evaluate the diversity of the thermal resistivity. The change of thermal capacity is governed by the crystal distribution of the XLPE. The physicochemical parameters of crystallinity (χ) and lamellar thickness (L) from DSC can be the indicator to evaluate the change of the thermal capacity. In addition, FWHM of the crystallization peak ΔW, crystalline rate index (T_0-T_P) and cross-linking degree (G) can also be the indicator of the thermal parameters. Finally, this paper proposes a more accurate on-line monitoring method for electric power industry by detecting thermal parameters to diagnose the operating cables in the practical application.

INDEX TERMS XLPE, cable, morphology, thermal resistivity, thermal capacity, cable ampacity, FTIR, DSC, cross-linking degree.

I. INTRODUCTION

Cross-linked polyethylene (XLPE) is playing an increasingly important role in high voltage cable insulation due to its high performance on electrical and thermal properties [1]–[3]. The insulating state (thermal history, operating period or material characteristic) of the XLPE has a profound effect on the safety and reliability of the cable operation because the external properties of the XLPE are determined directly by its morphology. It is found that [4] the accelerated aging process have damaged the crystal structure, which brought negative influence on the softening and melting temperature, resistivity, electrical breakdown, and dielectric losses of the XLPE. D. Andjelkovic and Rajakovic [5] have reported that mechanical properties, such as tensile strength and elongation-at-break, may associated with the crystallinity of the XLPE. It is pointed out that [6] different cross-linking degree has influence on crystal structure, resulting in different polarization index and volume resistivity of the XLPE. It is well evidenced that long-term actual operation of cable may change the morphology of XLPE insulation and result in degradation on the XLPE [7], [8]. Chemical composition of the XLPE may alter under different stresses over a period of time. Consequently, some of its properties may alter and produce limitation on the cable ampacity and diminution of effective service life for the cables [9].

Ampacity and aging mechanism are the most important topics for the cable practical operation, which should be given more comprehensive research. However, the aging factor is hard to define in the calculation of cable ampacity. Therefore, the precondition of cable ampacity calculation is setting the volumetric thermal capacity and thermal resistance of XLPE

The associate editor coordinating the review of this manuscript and approving it for publication was Giambattista Gruosso.

as fixed values [11], [12] in International Electrotechnical Commission (IEC) and Institute of Electrical and Electronics Engineers (IEEE) standards. From the perspective of dialectical materialism, nothing is immutable. Thus, it can be deduced preliminarily that the thermal parameters are fluctuating under different circumstances. In fact, previous research [13], [14] have found that the measured values of thermal resistance and thermal capacity of XLPE are different distinctly from the results of IEC standard. Moreover, it is reported that thermal parameters of the XLPE differ from the operating period of cables [9]. For the purpose of acquiring a better comprehension of the connection between cable ampacity and aging mechanism, it is meaningful to explore the potential connection between thermal parameters and insulating state of XLPE.

Currently, the assessment of XLPE insulating state by on-line monitoring technology in the actual operation cable line, such as detection of cable sheath circulating current and partial discharge, is lack of precision. There is an urgent need for a new on-line monitoring method to meet the requirement of transmission expansion [10]. In this case, it is of great significance to establish a more effective way to judge the XLPE insulating state and further estimate the remaining life of the operating cables. Therefore, it is imperative to quest for the relationship, changing tendency or regulation between morphology and thermal parameters of XLPE with different insulation states. Further, a new on-line monitoring method by detecting the changes of thermal parameters can be proposed. This will provide a more accurate way for electric power industry to diagnose the operating cables to pursue the optimized permissible long-term load capacity and extend their effective service life.

This paper has focused on two perspectives. The first perspective explores the correlation between the cable ampacity and thermal parameters of cable insulation. The second perspective concerns presentation of the results of the cables with different insulating states using several diagnostic measurements (FTIR, DSC, and Cross-linking degree) in order to reveal the correlation between the morphology and the thermal parameters of XLPE.

II. THEORETICAL ILLUSTRATION

Two important thermal parameters: thermal resistance and thermal capacity of XLPE, are vital for the accurate calculation of cable ampacity. Therefore, the following research mainly revolves around these two thermal parameters.

A. THE CORRELATION BETWEEN THE CABLE AMPACITY AND THERMAL PARAMETERS OF XLPE

The heat diffusion process from conductor core to surface of the XLPE cable can be simplified by thermal-circuit model [15]. The equivalent thermal circuit model of single core XLPE cables is depicted in Figure 1, which can reveal the correlation between cable ampacity and thermal parameters. Where P_0 denotes the losses of cable conductor;

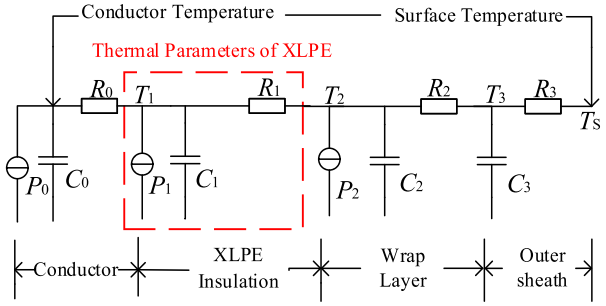

FIGURE 1. Equivalent transient thermal circuit model of single core XLPE cable.

P_1 denotes the dielectric losses of XLPE; P_2 denotes the losses of metal sheath, including the circulating current loss and the eddy-current loss; T_1 denotes the real-time surface temperature of cable conductor; T_2 denotes the real-time surface temperature of XLPE insulation; T_S denotes the real-time surface temperature of cable; R_0 denotes the thermal resistance of cable conductor; R_1 denotes the thermal resistance of XLPE insulation; R_2 denotes the thermal resistance of wrap layer; R_3 denotes the thermal resistance of outer sheath; C_0 denotes the heat capacity of cable conductor; C_1 denotes the heat capacity of XLPE insulation; C_2 denotes the heat capacity of wrap layer; C_3 denotes the heat capacity of outer sheath.

The cable ampacity is influenced directly by the thermal parameters of each layer, especially for the XLPE insulation with maximum consecutive portion within the cable. The fluctuation of thermal parameters within the XLPE layer may contribute to significant changes in cable ampacity. The following points can be summarized from the model.

1) The thermal resistance of XLPE signifies the ease of heat diffusion within the cable, that means the higher the R_1 is, the process of heat diffusion become more constricted. Consequently, the accumulative heat results particularly in the diminution of the cable ampacity in the equivalent conditions. Correspondingly, the lower the R_1 is, the permissible current can be lifted.
2) The volumetric thermal capacity of XLPE signifies the ability of thermal storage within the cable, that means the higher the C_1 is, the process of reaching steady-state temperature becomes more moderate. Therefore, the permissible transient current can be elevated in the equivalent conditions. Analogously, the lower the C_1 is, the permissible transient current should be declined.
3) The dielectric losses P_1 can be divided into two parts, including electrical conductive loss and the polarization loss. The dielectric losses are determined by the operating condition of the cable and the insulating state of XLPE. When the P_1 increases, more extra accumulative heat will be produced to lower the cable ampacity.

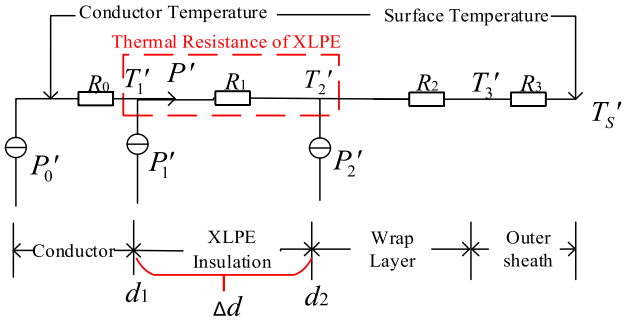

FIGURE 2. Equivalent steady thermal circuit model of single core XLPE cable.

B. THE THERMAL RESISTANCE AND THERMAL RESISTIVITY OF XLPE

Thermal resistance R_1 and thermal resistivity ρ_1 of XLPE possess the same characteristic in the aspect of heat conduction. The former is associated with the size and structure of the material and the latter is more inclined to the physical property of the material itself [16]. Therefore, the thermal resistivity ρ_1 is selected as the main study object in the subsequent research.

When the cable has reached the thermal steady state, the generated heat from the conductor will diffuse uniformly in the radial direction of the XLPE insulation, and the heat production is equal to the heat dissipation of the cable. For more detailed interpretation in the calculation of R_1 and ρ_1, the equivalent steady thermal circuit model of single core XLPE cable [18] is illustrated in Figure 2, where P_0' denotes the steady losses of cable conductor; P' denotes the general steady heat flow through the XLPE insulation; P_1' denotes the steady dielectric losses of XLPE; P_2' denotes the steady losses of metal sheath; T_1' denotes the real-time surface steady temperature of cable conductor; T_2' denotes the real-time surface steady temperature of XLPE insulation; T_S' denotes the real-time surface steady temperature of cable; d_1 denotes the radius of the conductor surface; d_2 denotes the radius of the XLPE insulation surface; and d denotes the thickness of the XLPE insulation. From Figure 2, R_1 and ρ_1 can be calculated as follows:

$$R_1 = \frac{T_1' - T_2'}{P'} \tag{1}$$

$$R_1 = \frac{\rho_1}{2\pi} \ln\left(\frac{d_2}{d_1}\right) \tag{2}$$

$$\rho_1 = \frac{2\pi(T_1' - T_2')}{P' \cdot \ln(d_2/d_1)} \tag{3}$$

where R_1 is thermal resistance (K · m/W); T_1' is the real-time surface steady temperature of cable conductor (K); T_2' is the real-time surface steady temperature of XLPE insulation (K); P' is the general steady heat flow through the XLPE insulation (W); ρ_1 is thermal resistivity of XLPE (K · m/W); d_1 is the radius of the conductor surface (mm) and d_2 is the radius of the XLPE insulation surface (mm).

TABLE 1. Critical parameters of the cables.

Cable	V_L	S_C	M_C	d_I	O_P
S1	110/64	500	Cu	17.5	30
S2	110/64	500	Cu	17.5	7
S3	110/64	500	Cu	17.5	3
S4	110/64	500	Cu	17.5	0
S5	110/64	630	Cu	16.5	0
S6	110/64	1600	Cu	16.0	0

V_L: voltage level in kV, S_C: conductor area in mm^2, M_C: conductor material, d_I: insulation thickness in mm, O_P: operation period in year.

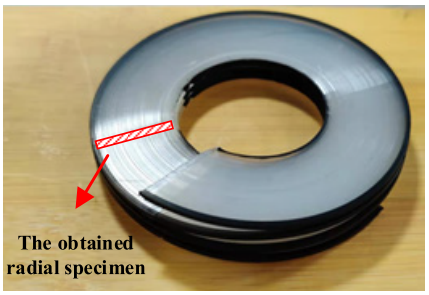

FIGURE 3. The obtained radial specimen from the experimental cable.

III. EXPERIMENT

A. PREPARATION OF XLPE SPECIMENS

Six HVAC XLPE cables with different insulating states were selected as the specimens in this paper. The critical information is listed in Table 1, where cable S1 to S3 are retired cables with the operating years of 30, 7 and 3; S4 to S6 are the spare cables with different specifications.

Each cable was peeled in the circumference direction of the conductor, and the tape-like XLPE peel with size of 160 × 5 × 0.5 mm were obtained as specimen shown in Figure 3, which can be considered as the specimen with average insulating state of the general XLPE insulation. These obtained specimens were all cleaned by alcohol to remove the surface impurities.

B. DIAGNOSTIC MEASUREMENTS OF XLPE PHYSICOCHEMICAL PARAMETERS

Fourier transform infrared spectroscopy (FTIR) measurement, differential scanning calorimetry (DSC) measurement and cross-linking degree measurement were adopted to obtain the physicochemical parameters of the specimens.

FTIR measurement: degradation and stability within the specimens were detected by the VERTEX 70 infrared spectrometer manufactured by German. Each specimen was tested at 32 scans in the range of 600∼3600 cm^{-1} with a resolution of 0.16 cm^{-1} and the signal-to-noise ratio of 55000:1. The obtained spectra were analyzed by OPUS software.

DSC measurement: crystal structure within the specimens were detected by the DSC NETZSCH-DSC 214 instrument manufactured by German. Specimens of 5 milligrams were

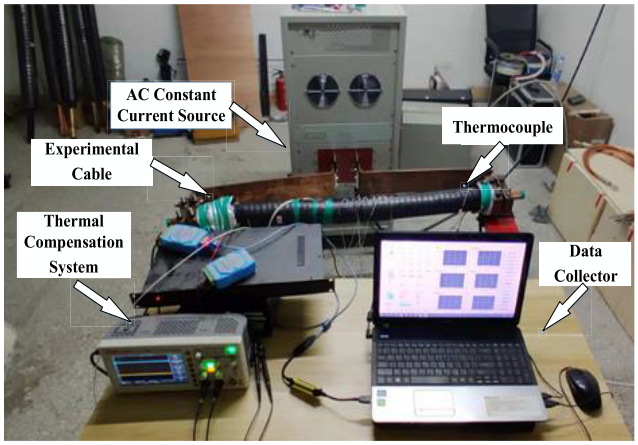

FIGURE 4. High-voltage cable thermal parameter detection control platform.

prepared to the test with the program of a heating phase and a cooling phase under nitrogen atmosphere to avoid thermal degradation. All specimens were heated from 25 to 140 °C at a rate of 10 °C /min and maintained at 140 °C for 5 min, and then cooled to 25 °C.

Cross-linking degree measurement: cross-linking degree of the specimens were determined by gel content. Specimens about 0.25 gram were prepared to detect the gel content of XLPE by using a solvent extraction method. Each specimen was placed in weighing bottle with xylene and extracted in forced air-circulating oven at 110 °C for 8 h. All specimens were then dried under vacuum at 150 °C for 30 min where upon a constant weight was reached. The weight of the cross-linked fraction that remained in was calculated by electronic balance, yielding the gel content of XLPE.

C. DIAGNOSTIC MEASUREMENTS OF XLPE THERMAL PARAMETERS

Thermal resistance and thermal resistivity measurement: the two parameters of XLPE insulation can be deduced inversely by means of the high-voltage cable thermal parameter detection control platform as illustrated in Figure 4. The details are as followed. Firstly, each cable with the length of 1.5 meters was installed in the experiment platform. Secondly, the thermocouples were installed on the surface of the conductor and the outer surface of the XLPE cable to monitor the temperature. Thirdly, steady conductor temperatures of the cable at 50, 70 and 90 °C were set and the corresponding steady AC currents were applied into the conductor. Fourthly, the parameters of T_1' and T_2' in Figure 2 can be measured from the temperature recorder of the platform, and the parameter of P' was approximately equal to P_0'due to R_0', P_1' and P_2' can be ignored comparing with P_0'. Fifthly, the parameters of R_1 and ρ_1 at 50, 70 and 90 °C were derived from Formula (1) and (3).

Specific heat capacity C_P measurement: the specific heat capacity C_P of the specimens can be detected by the DSC NETZSCH-DSC 214 instrument manufactured by German.

TABLE 2. The ampacity of the cables with the same specification under the air laying mode.

Specimen	θ_0 (°C)	θ_C (°C)	ρ_1 (K · m/W)	I_A (A)
S1	20	90	3.81	1098.1
S2	20	90	3.22	1172.4
S3	20	90	3.76	1103.9
S4	20	90	2.58	1272.8

θ_0: ambient temperature, θ_C: conductor steady-state temperature, ρ_1: thermal resistivity of XLPE and I_A: ampacity under the air laying mode.

The temperature was heated from 30 to 90 °C at a rate of 10 °C /min under the protective gas of nitrogen. Through the specific heat comparison method in the software of NETZCH-Proteus, the C_P-T spectra can be obtained.

IV. RESULTS AND DISCUSSION

The detecting ampacity of the cables with the same specification under the air laying mode was presented in Table 2. The change in thermal resistivity is predominant in the steady-state cable ampacity. It is found that the cable ampacity declined in S3 to S1 comparing with S4, which indicates the ampacity is influenced by the operated thermal history of the XLPE insulation. In this section, we have focused on the potential correlation between thermal parameters and physicochemical parameters of the XLPE with different insulating states.

A. RESULT OF XLPE PHYSICOCHEMICAL PARAMETERS MEASUREMENT

1) RESULT OF FTIR SPECTROSCOPY MEASUREMENT

Degradation and stability within the XLPE can be assessed from the FTIR spectra of the specimens as shown in Figure 5. The wavelength of 720 cm^{-1}, 1471 cm^{-1}, 2856 cm^{-1} and 2937 cm^{-1} are all caused by the vibration of the methylene band (-CH_2-). Due to the cross-linking process with the chemical agent of dicumyl peroxide (DCP), the decomposed products of acetophenone, cumyl alcohol and α-methylstyrene are generated within the XLPE. The functional groups of these chemicals are styryl, carbonyl (=C=O) and hydroxyl (-OH), which correspond to the absorption peaks at 1600 cm^{-1}, 1680 cm^{-1} and 3371 cm^{-1} [17] in Figure 5. Absorption peaks ranging from 1700 cm^{-1} to 1800 cm^{-1} can be considered as the thermo-oxidative products [22].

In Figure 5, significant differences of absorption peaks among the specimens are visible, suggesting the diversity of molecular structures. As regard to the retired cables of S3 to S1 comparing with S4, an intensive increase of the area over the range of 1600 to 1680 cm^{-1} with the increase of operation period. This result indicates the decomposition process on the backbone of the XLPE macromolecules becomes severer. Especially, the specimen of S1 presents a higher intensive peaks at 1600 cm^{-1}, 1680 cm^{-1} and 3371 cm^{-1}, indicating

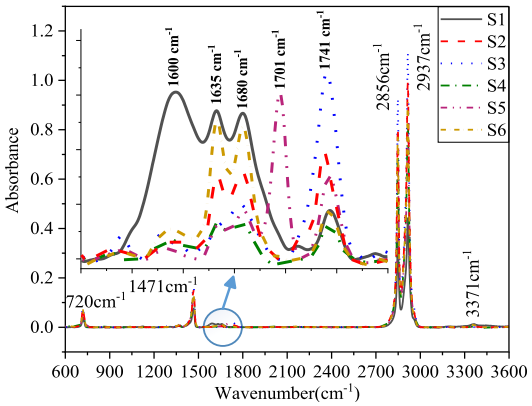

FIGURE 5. FTIR spectra of the specimens.

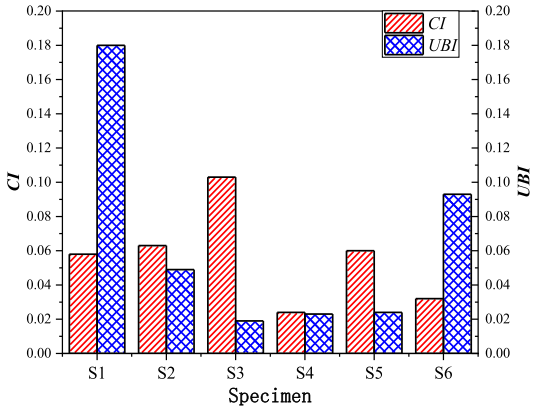

FIGURE 6. Carbonyl index (*CI*) and unsaturated band index (*UBI*) of the specimens.

the cross-linking process may occur during the long term practical operation with more cross-linking by-products. This opinion has been proven by the result of cross-linking degree measurement in the next section.

The XLPE insulating state of oxidation and decomposition can be judged by carbonyl index (*CI*) and unsaturated band index (*UBI*) from FTIR spectra. The definition of these two indexes are as followed [9]:

$$CI = I_{1741}/I_{1471} \tag{4}$$

$$UBI = I_{1635}/I_{1471} \tag{5}$$

where carbonyl index (*CI*) is the relative intensities of carbonyl band at 1741 cm^{-1} (aldehyde absorption) to the methylene band at 1471 cm^{-1}; unsaturated band index (*UBI*) is the relative intensities of unsaturated group at 1635 cm^{-1} to the methylene band at 1471 cm^{-1}. We have displayed the two indexes in Figure 6.

In Figure 6, it can be clearly observed that the *UBI* has increased with the increase of operation period. In this case, the chains decomposition is predominant in degradation within the XLPE. On the other aspect, distinct elevation in *CI* shows a severer oxidative process has occurred and the broken molecular chain segments are prone to transform into oxidative groups somehow, probably due to the overheating history.

TABLE 3. Cross-linking degree obtained from cross-linking degree measurement.

Specimen	W_1 (g)	W_2 (g)	G (%)
S1	0.2511	0.2165	86.2
S2	0.2468	0.2034	82.4
S3	0.2515	0.2191	87.1
S4	0.2479	0.2218	89.5
S5	0.2502	0.2229	89.1
S6	0.2497	0.2284	91.5

Although the chains decomposition (*UBI*) of S1 is accentuated, the carbonyl content (*CI*) is relatively low, which can be probably associated with the moderate condition during the cable operation. Due to the diversity in the manufacturing process of the spare cables, these two indexes are various in S4 to S6. S6 presents a higher *UBI*, reflecting the high concentrations of cross-linking byproducts within the XLPE, which means the relatively adequate cross-linking process has occurred in S6.

2) RESULT OF CROSS-LINKING DEGREE MEASUREMENT

After the cross-linking treatment of polyethylene (PE), three-dimensional network structure has been constructed within the PE molecular chain. The generated gel is hardly dissolve in most solvents. Gel content can be equivalent to the cross-linking degree, which is the relative weight of the insoluble portion after extraction to the original weight of the XLPE. The calculating process is given as follows [6]:

$$G(\%) = W_2/W_1 \times 100 \tag{6}$$

where G is gel content; W_1 is the original weight of the XLPE before extraction; and W_2 is the insoluble weight of the XLPE after extraction. The cross-linking degree of each specimen is shown in Table 3.

In Table 3, we can notice that S4 to S6 present higher cross-linking degree comparing with the S1 to S3, which is totally determined by the manufacturing step. With shorter operating period, the cross-linking degree for S3 and S2 has decreased progressively comparing with S4 due to the bond at the cross-link point was broken down. However, an abrupt elevation in cross-linking degree of S1 indicates the secondary cross-linking process has occurred during the long-term operation. This phenomenon is probably ascribed to the reaction of residual cross-linking agent within the XLPE during the operation.

3) RESULT OF DSC MEASUREMENT

For the results of DSC measurement, the thermos-gram of the heating phase is commonly used for observing the thermal history and the current crystal state, and the cooling phase can be analyzed on the ability to crystallize and the quality of the recrystallization [9]. Figure 7 shows the thermos-grams of the two phases of each specimen. Relevant parameters are listed in Table 4.

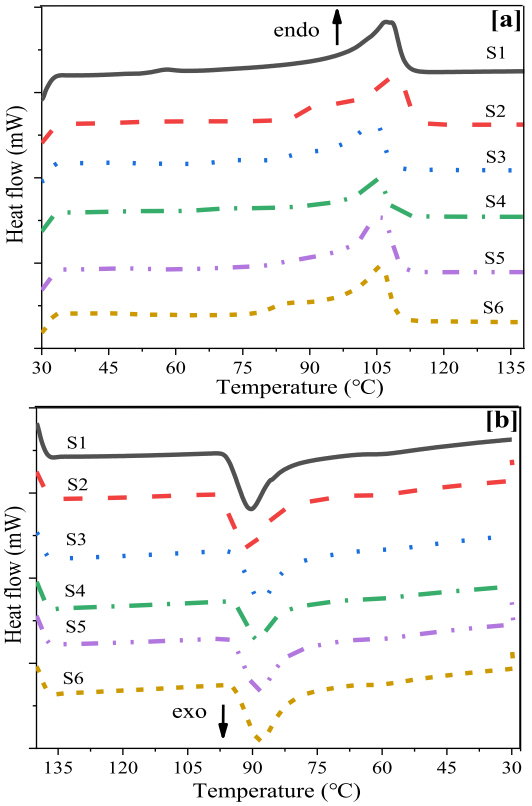

FIGURE 7. Heat flow as a function of measurement temperature in the heating phase and cooling phase of DSC. (a): Heating phase; (b): cooling phase.

TABLE 4. Parameters obtained from heating phase and cooling phase of DSC.

Specimen	T_m (°C)	ΔH_f (J/g)	R_m (°C)	T_0 (°C)	T_c (°C)	ΔH_c (J/g)
S1	107.0	115.0	15.7	95.9	90.3	-115.2
S2	108.9	117.8	13.6	97.6	90.8	-118.1
S3	104.6	98.1	11.8	93.9	88.0	-102.2
S4	105.0	79.7	10.0	93.9	88.9	-68.9
S5	106.1	108.2	12.6	94.6	88.4	-110.1
S6	105.8	107.2	13.3	94.2	88.0	-110.0

T_m—melting peak temperature, ΔH_f—enthalpy of fusion, R_m—melting range of the main endothermic peak, T_0—initial crystallizing temperature, T_c—crystallizing peak temperature, and ΔH_c—enthalpy of crystallization.

From Figure 7 (a), a small shoulder peak located at 50 to 90 ° C exists in most of the specimens expect for S4, which indicates the thermal history, causing by the degassing process during manufacture or overheating process during the actual operation of the cable [2]. For S4 to S1, it can be found that the melting range is widened with the increase of the operating period. This phenomenon can be ascribed to the generation of secondary crystals, which is commonly associated with the chain scission and formation of smaller chain segments. On the other hand, S4 to S6 with different specifications present the various DSC results due to the diversity of manufacturing process or the differences of the molecular chain and additives of the XLPE.

From Figure 7(b) and Table 4, it can be clearly observed that the cooling thermogram is associated with the operating period of cables. For S3 and S2, the exothermic peaks displace toward higher temperatures and the parameters of ΔH_c increases progressively comparing with S4, which indicated the improvement in crystal structure and expansion in crystal area. However, the recrystallization becomes deteriorated slightly for a long service time of S1 with the decrease of T_0, T_c and ΔH_c comparing with S2.

For the purpose to construct a solid correlation between the insulation morphology and thermal parameters of XLPE, more specific parameters are proposed in the following discussion. The DSC endotherms in Figure 7(a) indicate a range of melting process that can be related to the crystallinity and lamellar thickness variations. The detailed calculating formulas are as follows [9], [17]:

$$\chi(\%) = {\Delta H_f}\Big/{\Delta H_f^0} \times 100 \tag{7}$$

$$T_m = T_{m0}(1\text{-}{2\sigma_e}\Big/{\Delta H_m L}) \tag{8}$$

where $\chi(\%)$ is crystallinity; ΔH_f^0 is the enthalpy of fusion of an ideal polyethylene crystal per unit volume; T_m is the observed melting temperature (K); T_{m0} is the equilibrium melting temperature of an infinitely thick crystal; σ_e is the surface-free energy per unit area of basal face; ΔH_m is the enthalpy of fusion of an ideal polyethylene crystal per unit volume; and L is the lamellar thickness. The used values for calculation were as follows: $\Delta H_f^0 = 293$ J/g, $T_{m0} = 414,6$ K, $\Delta H_m = 2,88 \times 10^8$ J/m^3 and $\sigma_e = 93 \times 10^{-3}$ J/m^2.

In the study on non-isothermal melt-crystallization kinetics of polymers [19], the parameters of full width at half maximum (FWHM) of the crystallization peak ΔW and $(T_0\text{-}T_P)$ can be obtained from the DSC exotherms in Figure 7(b). ΔW is the measurement of the crystal size distribution, the lower the value is, the narrow distribution is. $(T_0\text{-}T_P)$ is the index which is proportional inversely to the recrystallization rate. The critical parameters from the heating phase and cooling phase are illustrated in Figure 8.

In Figure 8, it can be clearly observed that the changing trends of χ and L have coincided with ΔW *and*$(T_0\text{-}T_P)$ for all the specimens. Thus, these two couples of variables from the heating phase and cooling phase of DSC measurement can be extracted for the following research on the correlation between thermal parameters and physicochemical parameters of XLPE.

In Figure 8(a), significant increase in χ and L reflect improvement in the crystal structure of S3 and S2 comparing with S4. This phenomenon is attributed to the decrease of cross-linking degree and the generation of short chain segments during the practical operation, which activate adequate movement of the molecular chains to form the secondary crystal within the XLPE. Subsequently, the χ and

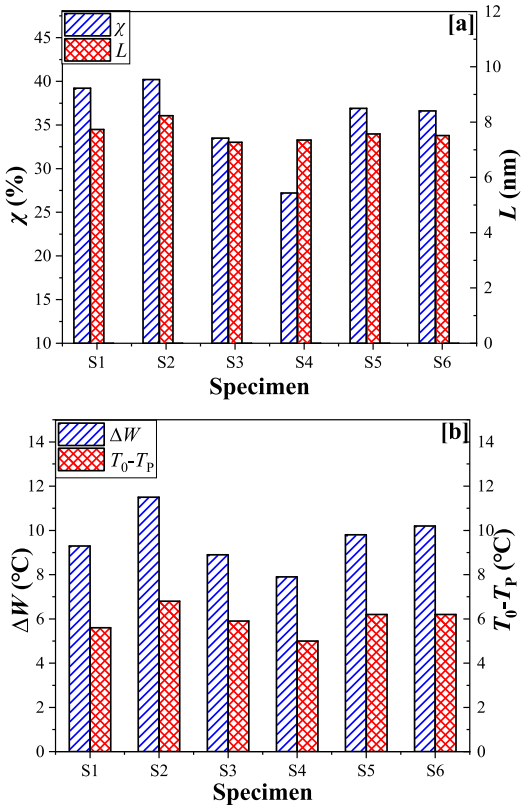

FIGURE 8. Critical parameters from the heating phase and cooling phase of DSC measurement. (a): crystallinity χ and lamellar thickness L; (b): full width at half maximum (FWHM) of the crystallization peak ΔW and index representing crystalline rate (T0-TP).

L have declined slightly in S1 due to the aggravation of deterioration for a long service time. Moreover, we can learn from Figure 8(b) that ΔW and $(T_0\text{-}T_P)$ have increased progressively in S3 and S2 comparing with S4, which means the crystal size distribution become wider and the recrystallization rate become moderate within the XLPE. The crystallization rate and crystal size distribution are governed by the growth rate of the grain and the generation rate of the crystal nucleus [8]. In this case, improvement of the recrystallization has occurred in S3 and S2. Relatively, ΔW and $(T_0\text{-}T_P)$ have decreased subsequently in S1, indicating that a slight deterioration has occurred in recrystallization after long service time of the cable.

On the aspect of the spare cables with different specifications, S5 and S6 show little diverseness in all the parameters from Figure 8, which indicates the similar initial crystal structure within the XLPE. However, S4 with lower χ and L presents inferior crystal structure comparing with S5 and S6, the diversity of which is mainly affected by the degassing process.

B. RESULT OF XLPE THERMAL PARAMETERS MEASUREMENT

1) RESULT OF THERMAL RESISTIVITY ρ MEASUREMENT

The thermal resistivity ρ of XLPE was calculated based on the measured temperatures in the high-voltage cable thermal parameter detection control platform. The obtained parameters of each cable were listed in Table 5.

TABLE 5. Thermal resistivity ρ (K · m/W) At 50, 70 and 90 °C of the cables.

T_c (°C)	S1	S2	S3	S4	S5	S6
50	3.22	3.12	3.29	2.45	2.43	2.36
70	3.67	3.19	3.51	2.51	2.35	2.43
90	3.81	3.22	3.76	2.58	2.59	2.67

Ideally, ρ is attribute of the material, which is barely relevant to the external factors, such as the size of the material or the change of temperature. However, the ρ of XLPE has increased progressively with the temperature increases shown in Table 5. This phenomenon is in accordance with the perspective of dialectical materialism about negative feedback. It is universally acknowledged that the cause of heat conduction is certainly impeded by the effect of heat conduction. Therefore, the increase in ρ definitely impedes the temperature rising process.

The diversity of ρ among the cables may be attributed to the change of crystal structure and molecular structure within the XLPE from the viewpoint of quantum theory [21]–[23]. The phonon heat conduction mechanism is associated with the anharmonicity of lattice vibration, which is governed by the grain size, grain boundaries and impurities within the XLPE.

The ρ has remained at lower values in regard to S4 to S6 with high cross-linking degree, which presents a high integrity and symmetry of molecular chains to decrease the anharmonicity of lattice vibration. Therefore, the increase of the mean free path of phonon scattering has finally improved the heat conduction of the cables. For S1 to S3, the ρ has been enlarged distinctly comparing with S4 to S6. Combining with the result of FTIR measurement, it is clearly observed that the total amount of *CI* and *UBI* coincides with the changes of ρ. With larger amount of *CI* and *UBI* of S1 to S3, the ρ becomes higher. Analogously, R_m from the result of DSC measurement reflects the same regulation. This phenomenon can be ascribed to the increase of polar groups and secondary crystals, which were formed during the practical operation of the cables. These substances aggravate the anharmonicity of lattice vibration within the XLPE, resulting in the increase of the ρ. On the other hand, the ρ of S2 is relatively low due to the small amount of micromolecular chain and the superior crystal structure within the XLPE. Therefore, the physicochemical parameters of *CI*, *UBI* and R_m can be the indicator to measure the anharmonicity of lattice vibration.

2) RESULT OF THERMAL CAPACITY C_P MEASUREMENT

XLPE is a high molecular polymer with crystal and amorphous phase and its crystal structure is governed by many factors, such as the cooling rate and the molecular chain structure. When the temperature decreases, the increased viscosity leads to the diminution in the mobility of chain segments.

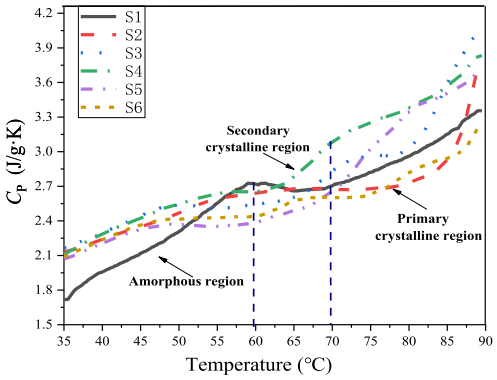

FIGURE 9. Specific heat capacity of the specimens.

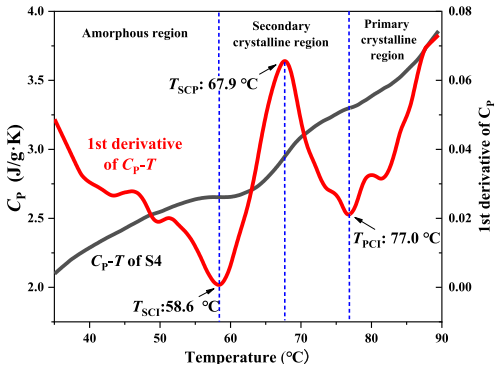

FIGURE 10. First derivative of the C_P-T curve of S4.

Therefore, the insufficient adjustment in the molecular chains results in the crystals with different stages within the XLPE, which have their own corresponding melting temperature.

From the DSC measurement, the C_P-T diagram of the specimens was obtained in Figure 9. The specific heat capacity C_P is the thermal parameter, reflecting the ability to store heat of XLPE. With the temperature increases, stepwise increase in C_P of each specimen can also be elaborated by dialectical materialism. The increase in C_P moderates the heating process so as to impede the rise of temperature, reflecting the negative feedback in the heat-transfer system. On the aspect of polymer physics, the changes in C_P indicates that the endothermic phenomenon occurs within the XLPE with the temperature increases. In lower measuring temperature range, a slight increase in C_P of each specimen is attributed to the melting process of amorphous region. Subsequently, the secondary crystals with poor morphological structure begin to melt as the temperature keeps rising, leading to a distinct increase in C_P. When the temperature exceeds a certain value, an abrupt lift in C_P of each specimen is particularly ascribed to the melting process of the primary crystals within the XLPE.

In order to distinguish the melting process in the different regions, first derivative of C_P-T is introduced to represent the melting rate of the specimens. Take S4 as an example in Figure 10, three regions (amorphous region, secondary crystalline region and primary crystalline region) can be divided according to the extremums of the first derivative of C_P-T. With the increasing of temperature, the amorphous region begins to melt slowly in the range of 30.0 to 58.6 °C. When the temperature exceeds 58.6 °C, the melting rate has a sudden rise at the range of 58.6 to 67.9 °C, and then decelerates at the range of 67.9 to 77.0 °C. This phase can be considered as melting process of secondary crystals. Finally, an abrupt elevation of melting rate occurs after 77.0 °C, which indicates the melting process of the primary crystals. Therefore, we can define three critical temperatures of T_{SCI}, T_{SCP} and T_{PCI} as an assessment of crystal structure. Where T_{SCI} is initial melting temperature in secondary crystalline area; T_{SCP} is the peak melting temperature in secondary crystalline area; and T_{PCI} is the initial melting temperatures in primary crystalline area. These parameters of each specimen were obtained in Table 6.

TABLE 6. Parameters obtained from C_P-T spectra with first derivative.

Specimen	T_{SCI} (°C)	T_{SCP} (°C)	T_{PCI} (°C)
S1	40.0	52.7	64.1
S2	49.0	75.9	81.4
S3	53.3	68.6	77.1
S4	58.6	67.9	77.0
S5	50.0	72.1	81.5
S6	58.4	77.9	84.1

T_{SCI}—initial melting temperature in secondary crystalline area, T_{SCP}—peak melting temperature in secondary crystalline area, and T_{PCI}—initial melting temperatures in primary crystalline area.

During the practical operation of the cables, the primary crystals of S3 and S2 are improved properly with higher melting temperature in the crystalline regions comparing with S4. In this process, a certain quantity of the imperfect crystals may be destroyed to form the crystals with more stable structure due to cold crystallization, which is responsible for the distinct increase in T_{SCP} and T_{PCI}. However, significant drop of T_{SCI}, T_{SCP} and T_{PCI} in S1 suggests the aggravation of deterioration in the crystal structure within the XLPE. On the other hand, we can notice that the initial crystal structure of the spare cables differs particularly from each other. It can be observed that there are three shoulder peaks occur in S5 and S6, indicating that different lengths of crystals that have their own corresponding melting temperature exist within the XLPE. This characteristic can be associated with the non-uniform distribution of crystals during the manufacturing process.

Since the C_P is associated with the melting process of the XLPE, related physicochemical parameters from the DSC measurement must be in light with the change of C_P. From the result of DSC measurement, it is found that χ and L are linked with the W *and* $(T_0$-$T_P)$. These parameters are the important indicator to evaluate the quality and distribution of the crystal structure. With higher χ and L, the crystal structure becomes more compact and thus the inflection points of the C_P-T

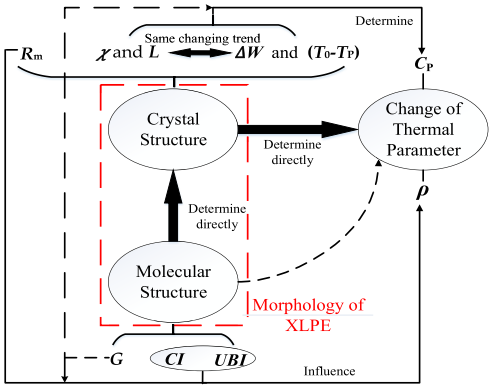

FIGURE 11. Correlation between thermal parameters and physicochemical parameters of XLPE. R_m: melting range; χ: crystallinity; L: lamellar thickness; ΔW: FWHM of the crystallization peak; $(T_0\text{-}T_P)$: index representing crystalline rate; G: crosslinking degree; CI: Carbonyl index; UBI: unsaturated band index; ρ: thermal resistivity; and C_P: specific heat capacity.

displace toward higher temperatures. In addition, the distribution of the crystal structure becomes more homogeneous with higher ΔW *and* $(T_0\text{-}T_P)$, leading to the inflection points appear at higher temperature in the C_P-T diagram as well. Therefore, it is reasonable to adopt these parameters as an indicator to measure the changes of the C_P.

C. CORRELATION BETWEEN THERMAL PARAMETERS AND PHYSICOCHEMICAL PARAMETERS OF XLPE

The fluctuation on thermal parameters of XLPE may be comprehended from the philosophical laws of natural evolution. Apart from a few mutations, the cause of the evolution process is always impeded by the effect in the evolution of natural phenomena. The cause of heat conduction is certainly impeded by the effect of heat conduction. For thermal resistivity ρ of XLPE, the value increases progressively with the temperature increases. In other words, the ascending thermal resistivity declines the heat conduction within the XLPE to impedes the elevation of temperature. Moreover, the aggravation of deterioration in the XLPE will lead to the increase in thermal resistivity, which in turn impedes the elevation of temperature to moderate the deterioration. Likewise, the thermal capacity C_P of XLPE increases progressively with the temperature increases in the range of 30∼90 °C due to the melting process of the crystal structure, indicating the heating process becomes mild to moderate the deterioration of the crystal structure within the XLPE.

Certainly, it is insufficient to interpret the fluctuation on thermal parameters of XLPE just through philosophical laws. The detailed interpretation must be in the light of the structural diversity of the XLPE. From the experimental results, the correlation between thermal parameters and physicochemical parameters of XLPE is presented in Figure 11.

From the viewpoint of quantum theory, the effect of lattice vibration is the main heat conduction mechanism of XLPE. The essence is thermally-excited phonons conduction, which is distinctly influenced by the anharmonicity of lattice vibration, such as the complexity of crystal structure and the defects within the XLPE. The increase in the anharmonicity of lattice vibration leads to higher thermal resistivity because of the shrinkage in mean free path of phonon scattering. Therefore, we can construct a correlation between the relevant physicochemical parameters and thermal resistivity from both the experiment and theory. From the results of the FTIR measurement, the increase in intensity of *UBI* or *CI* leads to the elevation of thermal resistivity. Similarly, the expansion of melting range from DSC measurement also results in the elevation of thermal resistivity.

On the other hand, the thermal capacity changing with temperature is associated with the melting process of crystal structure. With higher χ and L, the inflection points appear at higher temperature in the C_P-T diagram. Meanwhile, ΔW *and* $(T_0\text{-}T_P)$ are linked with the χ and L with the same changing trend, which can also be the evaluation indicator of thermal capacity.

It is noteworthy that cross-linking degree of XLPE is an important indicator for both thermal resistivity and thermal capacity, which can be closely related with microstructure and crystal structure. The high cross-linking degree restricts the mobility of molecular chains to hinder the further improvement of the crystal structure. Consequently, oxygen absorption and diffusion across the XLPE become easier, tending to generate more polar groups within the XLPE. Especially for the secondary cross-linking process during long-term operation, more tertiary hydrogen has been formed in the molecular structure of the XLPE, leading to the bond at the cross-link point is prone to be broken down. Take S1 for example, the *UBI* index increases and the crystal structure becomes deteriorate with the increase of the cross-linking degree. Therefore, high thermal resistivity and low thermal capacity can be deduced from the secondary cross-linking process.

V. CONCLUSION

The cable ampacity is determined by the thermal parameters of XLPE, which are closely related to the XLPE morphology. According to the results of the physicochemical and thermal parameters measurement, the following general conclusions can be made:

1) Steady-state ampacity of the cable is mainly influenced by thermal resistivity ρ, which is associated with the anharmonicity of lattice vibration. The physicochemical parameters of the carbonyl index *CI* and unsaturated band index *UBI* from FTIR measurement and the melting range Rm from DSC measurement can be the indicator to evaluate the diversity of the ρ. With the increase of the *CI* and *UBI* and expansion of the R_m, the ρ becomes higher.
2) Transient heating process of the cable is mainly influenced by thermal capacity C_P, which is associated with the crystal distribution of the XLPE. The physicochemical parameters of the crystallinity χ and thicker

lamellae L from DSC measurement can be the indicator to evaluate the change of the C_P. With higher χ and L, the inflection points appear at higher temperature in the C_P-T diagram.

3) Other physicochemical parameters, such as FWHM of the crystallization peak ΔW, crystalline rate index (T_0-T_P) and cross-linking degree G can also be the indicator to evaluate the thermal parameters.

In the future, more work will be devoted to reveal the potential correlation between the morphology and the thermal parameters of XLPE to propose a new on-line monitoring method by detecting the thermal parameters. In this way, we can diagnose the XLPE insulating state directly and establish relevant strategies to prolong the cable service life and further estimate its remaining life.

ACKNOWLEDGMENT

(Yifeng Zhao and Zhuozhan Han contributed equally to this work.)

REFERENCES

[1] Y. Xie, G. Liu, Y. Zhao, L. Li, and Y. Ohki, "Rejuvenation of retired power cables by heat treatment," *IEEE Trans. Dielectr. Electr. Insul.*, vol. 26, no. 2, pp. 668–670, Apr. 2019.

[2] Y. Xie, Y. Zhao, S. Bao, P. Wang, J. Huang, P. Wang, G. Liu, Y. Hao, and L. Li, "Investigation on cable rejuvenation by simulating cable operation," *IEEE Access*, vol. 8, pp. 6295–6303, 2020.

[3] Y. Xie, Y. Zhao, S. Bao, P. Wang, J. Huang, G. Liu, Y. Hao, and L. Li, "Rejuvenation of retired power cables by heat treatment: Experimental simulation in lab," *IEEE Access*, vol. 8, pp. 5635–5643, 2020.

[4] S. Grzybowski, P. Zubielik, and E. Kuffel, "Changes of thermoplastic PE cable insulation properties caused by the overload current," *IEEE Trans. Power Del.*, vol. 4, no. 3, pp. 1507–1512, Jul. 1989.

[5] D. Andjelkovic and N. Rajakovic, "Influence of accelerated aging on mechanical and structural properties of cross-linked polyethylene (XLPE) insulation," *Electr. Eng.*, vol. 83, nos. 1–2, pp. 83–87, Feb. 2001.

[6] R. Polansky, M. Cermak, and M. Bartunkova, "A comparative study of dielectric, mechanical and structural properties of fire-protective insulation based on XLPE," in *Proc. IEEE Int. Conf. Solid Dielectr. (ICSD)*, Bologna, Italy, Jun. 2013, pp. 674–677.

[7] L. Boukezzi, A. Boubakeur, C. Laurent, and M. Lallouani, "Observations on structural changes under thermal ageing of cross-linked polyethylene used as power cables insulation," *Iranian Polym. J.*, vol. 17, no. 8, pp. 611–624, Aug. 2008.

[8] H. Li, J. Li, Y. Ma, Q. Yan, and B. Ouyang, "The role of thermo-oxidative aging at different temperatures on the crystal structure of crosslinked polyethylene," *J. Mater. Sci., Mater. Electron.*, vol. 29, no. 5, pp. 3696–3703, Mar. 2018.

[9] W. W. Zhu, Y. F. Zhao, Z. Z. Han, X. B. Wang, Y. F. Wang, and G. Liu, "Thermal effect of different laying modes on cross-linked polyethylene (XLPE) insulation and a new estimation on cable ampacity," *Energies*, vol. 12, no. 15, p. 2994, Aug. 2019.

[10] Z. Liang, H. Chen, S. Chen, Z. Lin, and C. Kang, "Probability-driven transmission expansion planning with high-penetration renewable power generation: A case study in northwestern China," *Appl. Energy*, vol. 255, Dec. 2019, Art. no. 113610.

[11] P. Wang, G. Liu, H. Ma, Y. Liu, and T. Xu, "Investigation of the ampacity of a prefabricated straight-through joint of high voltage cable," *Energies*, vol. 10, no. 12, p. 2050, Dec. 2017.

[12] X.-K. Meng, Z.-Q. Wang, and G.-F. Li, "Dynamic analysis of core temperature of low-voltage power cable based on thermal conductivity," *Can. J. Electr. Comput. Eng.*, vol. 39, no. 1, pp. 59–65, 2016.

[13] Y. J. Han, H. M. Lee, and Y.-J. Shin, "Thermal aging estimation with load cycle and thermal transients for XLPE-insulated underground cable," in *Proc. IEEE Conf. Electr. Insul. Dielectric Phenomenon (CEIDP)*, Oct. 2017, pp. 205–208.

[14] X. Cao, Z. Yi, K. Chen, X. Zhang, and J. Yang, "Laying mode and laying spacing for single-core feeder cable of high speed railway," *China Railway Sci.*, vol. 36, no. 6, pp. 85–90, Nov. 2015.

[15] C. Lei, G. Liu, B. Ruan, and Y. Liu, "Experimental research of dynamic capacity based on conductor temperature-rise characteristic of HV single-core cable," *High Voltage Eng.*, vol. 38, no. 6, pp. 1397–1402, Jun. 2012.

[16] Z. Han, G. Liu, P. Wang, T. Xu, and Y. Liu, "Determination method for optimal hierarchy numbers of insulation layer in transient thermal circuit of high-voltage cable," *Guangdong Electr. Power*, vol. 30, no. 10, pp. 28–34, Oct. 2017.

[17] J. Karger-Kocsis, "Thermal analysis of polymers: Fundamentals and applications," *Macromol. Chem. Phys.*, vol. 210, no. 19, p. 1661, Oct. 2009.

[18] T. Salivon, X. Colin, and R. Comte, "Degradation of XLPE and PVC cable insulators," in *Proc. IEEE Conf. Elect. Insul. Dielectr. Phenomena (CEIDP)*, Ann Arbor, MI, USA, Oct. 2015, pp. 656–659.

[19] L. Boukezzi, A. Boubakeur, and M. Lallouani, "Effect of artificial thermal aging on the crystallinity of XLPE insulation cables: X-ray study," in *Proc. Annu. Rep.-Conf. Elect. Insul. Dielectr. Phenomena*, Vancouver, BC, Canada, Oct. 2007, pp. 65–68.

[20] A. K. Gupta and S. N. Purwar, "Crystallization of PP in PP/SEBS blends and its correlation with tensile properties," *J. Appl. Polym. Sci.*, vol. 29, no. 5, pp. 1595–1609, May 1984.

[21] A. V. Kostanovskiy, M. E. Kostanovskaya, and M. G. Zeodinov, "About a phonon mechanism of heat conduction in graphite at high temperatures," *High Temp.*, vol. 51, no. 3, pp. 426–429, May 2013.

[22] T. Zeng and G. Chen, "Phonon heat conduction in thin films: Impacts of thermal boundary resistance and internal heat generation," *J. Heat Transf.*, vol. 123, no. 2, pp. 340–347, Apr. 2001.

[23] G. Chen, "Phonon heat conduction in nanostructures1," *Int. J. Therm. Sci.*, vol. 39, no. 4, pp. 471–480, Apr. 2000.

YIFENG ZHAO received the B.Eng. degree in electrical engineering from Qingchuan University, Wuhan, China, in 2017. He is currently pursuing the M.Eng. degree in electrical engineering with the South China University of Technology, Guangzhou, China. His research interests include degradation mechanism of polymer dielectric materials and aging assessment of XLPE cable.

ZHUOZHAN HAN received the B.Sc.(Engg.) degree in electrical engineering from the South China University of Technology, Guangzhou, China, in 2017, where he is currently pursuing the M.Eng. degree in electrical engineering. His research interest includes ampacity assessment of power cable.

YUE XIE received the B.Eng. degree in electrical engineering from Wuhan Polytechnic University, Wuhan, China, in 2013. He is currently pursuing the Ph.D. degree in electrical engineering with the South China University of Technology, Guangzhou, China. His research interests include degradation mechanism of polymer dielectric materials and aging assessment of XLPE cable.

XINGHUI FAN received the B.Eng. degree in electrical engineering from Fuzhou University, Fuzhou, China, in 2019. He is currently the M.Eng. degree in electrical engineering with the South China University of Technology, Guangzhou, China. His current researches focus on the polymer dielectric materials and aging assessment of XLPE cable.

YANGYANG NIE received the B.Eng. degree in electrical engineering from Zhengzhou University, Zhengzhou, China, in 2019. He is currently pursuing the M.Eng. degree in electrical engineering with the South China University of Technology, Guangzhou, China. His current research focuses on the corona plasama treatment on the surface of PVDF.

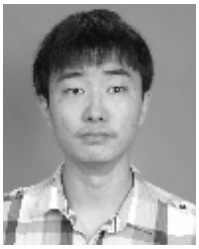

PENGYU WANG received the B.Sc.(Engg.) degree in electrical engineering from the South China University of Technology, Guangzhou, China, in 2016, where he is currently pursuing the Ph.D. degree in electrical engineering. His research interests include ampacity assessment and fault diagnosis of power cable.

GANG LIU (Member, IEEE) received the B.Eng., M.Eng., and Ph.D. degrees in electrical engineering from Xi'an Jiaotong University, Xi'an, China, in 1991, 1994, and 1998, respectively. He is currently an Associate Professor with the School of Electric Power, South China University of Technology, Guangzhou, China. His research interests include ampacity assessment and fault diagnosis of electrical equipment and lightning protection of transmission line.

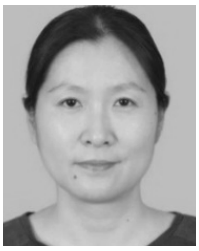

YANPENG HAO (Member, IEEE) was born in Hebei, China, in 1974. She received the M.Sc. and Ph.D. degrees in electrical engineering from Xi'an Jiaotong University, China, in 1998 and 2003, respectively. She is currently a Professor with the South China University of Technology, China. Her major research fields are insulation condition monitoring and life evaluation of electrical power equipment, insulation performance of UHV/EHV transmission lines under lighting, icing, and pollution.

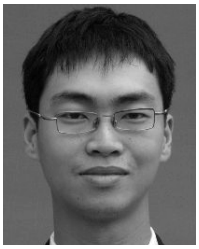

JIASHENG HUANG received the B.Eng. degree in electrical engineering from the Guangdong University of Technology, Guangzhou, China, in 2004. Since 2004, he has been an Engineer with Guangzhou Power Supply Company, Ltd., Guangzhou. His research interest is failure diagnose of transmission cables.

WENWEI ZHU received the master's degree in electrical engineering from Xi'an Jiaotong University, Xi'an, China, in 2008. Since 2008, he has been an Engineer with Guangdong Power Grid Corporation, Guangzhou, China. His research interest is transmission cables.